Journal of Computational and Applied Mathematics 233 (2010) 2737–2754

Contents lists available at ScienceDirect

Journal of Computational and Applied Mathematics

journal homepage: www.elsevier.com/locate/cam

Meshless local Petrov–Galerkin (MLPG) approximation to the two dimensional sine-Gordon equation

Davoud Mirzaei, Mehdi Dehghan *

Department of Applied Mathematics, Faculty of Mathematics and Computer Science, Amirkabir University of Technology, No. 424, Hafez Avenue, 15914, Tehran, Iran

ARTICLE INFO

Article history:
Received 22 June 2009
Received in revised form 8 November 2009

MSC:
65M Except 65M06
65M12
65M15
65M20

Keywords:
Meshless local Petrov–Galerkin (MLPG) method
Moving least-squares (MLS) approximation
Sine-Gordon (SG) equation

ABSTRACT

During the past few years, the idea of using meshless methods for numerical solution of partial differential equations (PDEs) has received much attention throughout the scientific community, and remarkable progress has been achieved on meshless methods. The meshless local Petrov–Galerkin (MLPG) method is one of the "truly meshless" methods since it does not require any background integration cells. The integrations are carried out locally over small sub-domains of regular shapes, such as circles or squares in two dimensions and spheres or cubes in three dimensions. In this paper the MLPG method for numerically solving the non-linear two-dimensional sine-Gordon (SG) equation is developed. A time-stepping method is employed to deal with the time derivative and a simple predictor–corrector scheme is performed to eliminate the non-linearity. A brief discussion is outlined for numerical integrations in the proposed algorithm. Some examples involving line and ring solitons are demonstrated and the conservation of energy in undamped SG equation is investigated. The final numerical results confirm the ability of proposed method to deal with the unsteady non-linear problems in large domains.

1. Introduction

The finite element method (FEM) and the closely related finite volume method are well-established numerical techniques for computer modelling in engineering and science. However, these and other mesh-based methods possess several shortcomings due to their reliance on a mesh. The generation of quality meshes presents significant difficulties in the analysis of many engineering components. Attempts to overcome these difficulties have been made through the development of meshless methods which have attracted considerable interest over the past decade. The primary objective of meshless methods is to eliminate, or at least alleviate, the difficulty of meshing by defining the problem domain discretization using only nodes and a description of the problem domain boundary. Recent advances in the mesh-free techniques for solving partial differential equations (PDEs) of physics and engineering have enabled reliable modelling of phenomena that pose considerable challenges to the traditional mesh-based techniques. This great benefit comes at a price of more complicated interpolation functions and subsequent difficulties with implementing efficient integration schemes, among other problems. Meshless methods such as the element-free Galerkin [1], hp-clouds [2], the reproducing kernel particle [3], the smoothed particle hydrodynamics [4], the diffuse element [5], the partition of unity finite element [6], the natural element [7] and etc. for seeking approximate solutions of partial differential equations have become popular during the last two decades because of the flexibility of placing nodes at arbitrary locations and the ability to treat the evolution of many engineering problems. Many of these methods employ basis functions obtained by the moving least-squares (MLS) technique in [8] to

* Corresponding author. Fax: +98 21 66497930.
E-mail addresses: d_mirzaei@aut.ac.ir (D. Mirzaei), mdehghan@aut.ac.ir, mdehghan.aut@gmail.com, mdehghan_aut@yahoo.com (M. Dehghan).

0377-0427/$ – see front matter © 2009 Elsevier B.V. All rights reserved.
doi:10.1016/j.cam.2009.11.022

approximate the trial solution, and a background mesh to numerically evaluate integrals appearing in the weak formulation of a problem. The above-mentioned methods are all based on a global weak form, being "meshless" only in terms of the interpolation of the field variables. Most meshless methods have to use background cells to integrate a weak form over the problem domain. The requirement of background cells for integration makes the methods not "truly" meshless. Recently a method based on local sub-domains, rather than a global problem domain, was introduced by Atluri and his colleagues. A truly meshless method, called the Meshless Local Petrov–Galerkin (MLPG) method, was first proposed in [9], and later discussed in depth in [10,11]. In the MLPG method no background mesh is used to evaluate integrals appearing in the local weak formulation of the problem. The MLPG is a relatively new class of meshless method in which the weak form equations are satisfied locally in sub-domains that surround each node. In this method, a nodal sub-domain is constructed to facilitate the local integration of the weak form equations and is used in place of background integration cells. Since no globally defined integration structure is required, the MLPG method has been referred to as a truly meshless method and has been successfully applied for the solution of a wide range of problems in engineering and science [12–19].

In this work, application of the MLPG method is used for the analysis of non-linear two-dimensional sine-Gordon (SG) equation.

Over the last two decades, some attentions have been paid to models which possess soliton-like structures in higher dimensions. Soliton solutions have been found in a variety of non-linear differential equations such as the Korteweg and de Vries (KdV) equation, the Schrödinger equation [20], the sine-Gordon equation, etc. Physical applications of solitons have been found among others in shallow-water waves, optical fibers, Josephson junction oscillators, etc. In particular, the Josephson junction model which consists of two layers of superconducting material separated by an isolating barrier (see [21,22]). This model is found to have many applications in electronics and can be described by the two-dimensional undamped sine-Gordon equation. Moreover, it is found to possess soliton-like solutions [23–26].

Consider the two-dimensional sine-Gordon equation

$$\frac{\partial^2 u}{\partial t^2} + \beta \frac{\partial u}{\partial t} = \frac{\partial^2 u}{\partial x^2} + \frac{\partial^2 u}{\partial y^2} - \psi(x, y) \sin(u), \quad (x, y) \in \Omega,\ t \geq 0, \tag{1.1}$$

where $\Omega = \{(x, y) | a \leq x \leq b, c \leq y \leq d\}$. The boundary conditions associated with (1.1) impose a zero gradient along the boundary Γ of Ω

$$\frac{\partial u}{\partial n}(x, y, t) = 0, \quad (x, y) \in \Gamma,\ t \geq 0, \tag{1.2}$$

while the initial conditions are given by

$$u(x, y, 0) = f(x, y), \quad (x, y) \in \Omega \tag{1.3}$$

and

$$\frac{\partial u}{\partial t}(x, y, 0) = g(x, y), \quad (x, y) \in \Omega. \tag{1.4}$$

The function $\psi(x, y)$ can be interpreted as a Josephson current density, and $f(x, y)$ and $g(x, y)$ are wave modes or kinks and velocity, respectively. The parameter β is the so-called dissipative term, which is assumed to be a real number with $\beta \geq 0$. When $\beta = 0$, Eq. (1.1) reduces to the undamped SG equation in two space variables, while when $\beta > 0$, to the damped one.

For the undamped SG equation in higher dimensions the exact soliton solutions have obtained in [27] using Hirota's method, in [28,29] using Lamb's method, in [30] by Painlevè transcendents and in [31] by Bläcklund transformation, etc. Numerical solutions for the SG equation have given in [32] using two difference schemes, Christiansen and Lomdahl [26] using a generalized leapfrog method, Argyris et al. [23] by the finite element approach, Sheng et al. [33] by a split cosine scheme, Djidjeli et al. [25] using a two-step one-parameter leapfrog scheme, Bratsos [34] using a three time level fourth order explicit finite-difference scheme, Bratsos [35] using a modified predictor–corrector scheme, Bratsos [24] using the method of lines, Bratsos [36] by a third order numerical scheme, Bratsos [37] using a rational approximant of order 4, which is applied to a three time level recurrence relation, Dehghan and Mirzaei [38] by the dual reciprocity boundary element approximation, Mirzaei and Dehghan [39] using continuous linear boundary elements, Dehghan and Shokri [40] using the radial basis functions, and etc. Also the one-dimensional SG equation has been considered widely in numerical and exact solutions. For example see [41–43] and the references therein. In this work we focus on the two-dimensional SG soliton-like solutions. For soliton solutions of partial differential equation we refer the interested reader to the review paper of [44].

The remainder of the paper is organized as follows: In Section 2, the local weak form is outlined for the SG equation. In Section 3, a brief discussion of MLS is presented. In Section 4, the discretized equations are extracted, a predictor–corrector method is explained and the numerical integrations are performed. In Section 5, numerical results for some problems, involving line and ring solitons, are investigated and the reformations of the solitons from initial condition to final time are given. Also to test the accuracy of the proposed method the value of energy at several time-steps are computed. Finally in Section 6 the report ends with a brief conclusion.

2. The MLPG formulation

2.1. The time difference approximation

In the MLPG method to deal with the time derivative we can apply the Laplace transform or use a time-stepping approximation. Algorithms for the numerical inversion of a Laplace transform lead to a reduction in accuracy. Also the Laplace transform could not applied to the non-linear equations. Consequently, we employ a time-stepping method to overcome the time derivatives in this equation. For this purpose, the following approximations can be used

$$\begin{aligned}
&\frac{\partial^2 u}{\partial t^2}(\mathbf{x},t) \simeq \frac{1}{(\Delta t)^2}\left[u^{(k+1)}(\mathbf{x}) - 2u^{(k)}(\mathbf{x}) + u^{(k-1)}(\mathbf{x})\right],\\
&\frac{\partial u}{\partial t}(\mathbf{x},t) \simeq \frac{1}{2\Delta t}\left[u^{(k+1)}(\mathbf{x}) - u^{(k-1)}(\mathbf{x})\right],\\
&u(\mathbf{x},t) \simeq \frac{1}{3}\left[u^{(k+1)}(\mathbf{x}) + u^{(k)}(\mathbf{x}) + u^{(k-1)}(\mathbf{x})\right],
\end{aligned} \tag{2.1}$$

where $u^{(k)}(\mathbf{x}) = u(\mathbf{x}, k\Delta t)$ and $\mathbf{x} = (x, y)$. To deal with the non-linearity, we adopt an iterative approach. $\sin(u)$ is estimated by $\sin(\widetilde{u})$, where $\widetilde{u}$ is the latest available approximation of u, as will be described in Section 4.2. Using (2.1) and above discussions, Eq. (1.1) can be written as

$$\frac{1}{3}\nabla^2 u^{(k+1)} - (\eta+\alpha)u^{(k+1)} = -\frac{1}{3}\nabla^2 u^{(k)} - 2\alpha u^{(k)} - \frac{1}{3}\nabla^2 u^{(k-1)} - (\eta-\alpha)u^{(k-1)} + \psi(\mathbf{x})\sin(\widetilde{u}), \tag{2.2}$$

where $\alpha = 1/(\Delta t)^2$ and $\eta = \beta/(2\Delta t)$.

2.2. The local weak form

Instead of giving the global weak form for Eq. (2.2), the MLPG method constructs the weak form over local sub-domains such as Ω_s, which is a small region taken for each node in the global domain Ω. The local sub-domains overlap each other, and cover the whole global domain Ω. The local sub-domains could be of any geometric shape and size. For simplicity they are taken to be of circular shape. The local weak form of the approximate equation (2.2) for $\mathbf{x} \in \Omega_s^i$ can be written as

$$\begin{aligned}
&\int_{\Omega_s^i}\left[\frac{1}{3}\nabla^2 u^{(k+1)} - (\eta+\alpha)u^{(k+1)}\right]u^*(\mathbf{x})\mathrm{d}\Omega = -\int_{\Omega_s^i}\left[\frac{1}{3}\nabla^2 u^{(k)} + 2\alpha u^{(k)}\right]u^*(\mathbf{x})\mathrm{d}\Omega\\
&\quad - \int_{\Omega_s^i}\left[\frac{1}{3}\nabla^2 u^{(k-1)} + (\eta-\alpha)u^{(k-1)}\right]u^*(\mathbf{x})\mathrm{d}\Omega + \int_{\Omega_s^i}\psi(\mathbf{x})\sin(\widetilde{u})u^*(\mathbf{x})\mathrm{d}\Omega,
\end{aligned} \tag{2.3}$$

where u^* is a test function. Using

$$[\nabla^2 u]u^* = u_{,ll}u^* = [u_{,l}u^*]_{,l} - u_{,l}u^*_{,l},$$

and the divergence theorem, Eq. (2.3) yields the following expression

$$\begin{aligned}
&\frac{1}{3}\left[\int_{\partial\Omega_s^i} u_{,l}^{(k+1)} n_l u^* \mathrm{d}\Gamma - \int_{\Omega_s^i} u_{,l}^{(k+1)} u^*_{,l}\mathrm{d}\Omega\right] - (\eta+\alpha)\int_{\Omega_s^i} u^{(k+1)}u^*\mathrm{d}\Omega\\
&\quad = -\frac{1}{3}\left[\int_{\partial\Omega_s^i} u_{,l}^{(k)} n_l u^* \mathrm{d}\Gamma - \int_{\Omega_s^i} u_{,l}^{(k)} u^*_{,l}\mathrm{d}\Omega\right] - 2\alpha\int_{\Omega_s^i} u^{(k)}u^*\mathrm{d}\Omega - \frac{1}{3}\left[\int_{\partial\Omega_s^i} u_{,l}^{(k-1)} n_l u^* \mathrm{d}\Gamma - \int_{\Omega_s^i} u_{,l}^{(k-1)} u^*_{,l}\mathrm{d}\Omega\right]\\
&\qquad - (\eta-\alpha)\int_{\Omega_s^i} u^{(k-1)}u^*\mathrm{d}\Omega + \int_{\Omega_s^i}\psi(\mathbf{x})\sin(\widetilde{u})u^*\mathrm{d}\Omega,
\end{aligned} \tag{2.4}$$

where Ω_s^i is a local sub-domain associated with the point i, i.e., it is a circle centered at $\mathbf{x}^i$ of radius r_0, and $\partial\Omega_s^i$ is the boundary of Ω_s^i.

If the Heaviside step function

$$u^*(\mathbf{x}) = \begin{cases} 1, & \mathbf{x} \in \Omega_s,\\ 0, & \mathbf{x} \notin \Omega_s, \end{cases} \tag{2.5}$$

is chosen as the test function in each sub-domain [45,46], then the local weak form (2.4) is transformed into the following simple local integral equation

$$\begin{aligned}
\frac{1}{3}\int_{\partial\Omega_s^i} u_{,l}^{(k+1)} n_l \mathrm{d}\Gamma - (\eta+\alpha)\int_{\Omega_s^i} u^{(k+1)}\mathrm{d}\Omega &= -\frac{1}{3}\int_{\partial\Omega_s^i} u_{,l}^{(k)} n_l u^*\mathrm{d}\Gamma - 2\alpha\int_{\Omega_s^i} u^{(k)}\mathrm{d}\Omega - \frac{1}{3}\int_{\partial\Omega_s^i} u_{,l}^{(k-1)} n_l \mathrm{d}\Gamma\\
&\quad - (\eta-\alpha)\int_{\Omega_s^i} u^{(k-1)}\mathrm{d}\Omega + \int_{\Omega_s^i}\psi(\mathbf{x})\sin(\widetilde{u})\mathrm{d}\Omega.
\end{aligned} \tag{2.6}$$

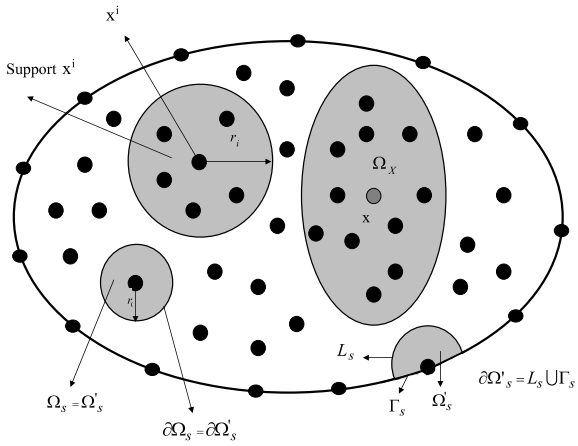

Fig. 1. Local boundaries and the domain of definition of MLS approximation.

For boundary points according to Fig. 1, $\partial\Omega_s^i$ and Ω_s^i replaced by $L_s^i \bigcup \Gamma_s^i$ and $\Omega_s^{\prime i}$ respectively. i.e. we have

$$\frac{1}{3}\int_{L_s^i} u_{,l}^{(k+1)} n_l \mathrm{d}\Gamma + \frac{1}{3}\int_{\Gamma_s^i} u_{,l}^{(k+1)} n_l \mathrm{d}\Gamma - (\eta+\alpha)\int_{\Omega_s^{\prime i}} u^{(k+1)} \mathrm{d}\Omega = -\frac{1}{3}\int_{L_s^i} u_{,l}^{(k)} n_l \mathrm{d}\Gamma - \frac{1}{3}\int_{\Gamma_s^i} u_{,l}^{(k)} n_l \mathrm{d}\Gamma$$
$$-2\alpha\int_{\Omega_s^{\prime i}} u^{(k)} \mathrm{d}\Omega - \frac{1}{3}\int_{L_s^i} u_{,l}^{(k-1)} n_l \mathrm{d}\Gamma - \frac{1}{3}\int_{\Gamma_s^i} u_{,l}^{(k-1)} n_l \mathrm{d}\Gamma - (\eta-\alpha)\int_{\Omega_s^{\prime i}} u^{(k-1)} \mathrm{d}\Omega + \int_{\Omega_s^{\prime i}} \psi(\mathbf{x}) \sin(\widetilde{u}) \mathrm{d}\Omega. \tag{2.7}$$

Applying a spatial approximation for the unknown functions, the local integral equations (2.6) and (2.7) are transformed in to a system of algebraic equations with real unknown quantities at nodes used for spatial approximation, as described in the next section.

3. The MLS approximation

To solve the local integral equations (2.6) and (2.7) numerically, a meshless method based on the moving least-squares (MLS) scheme is adopted. The MLS scheme [47,8] represents one of many interpolation methods known in literature. Let us consider a sub-domain $\Omega_{\mathbf{x}}$ of Ω in the neighbourhood of a point $\mathbf{x}$ for the definition of the MLS approximation of the trial function around $\mathbf{x}$. To approximate the distribution of the function $u^{(k)}(\mathbf{x})[=u(\mathbf{x}, k\Delta t)]$ in $\Omega_{\mathbf{x}}$, over a number of randomly located nodes $\{\mathbf{x}^i\}$, $i = 1, 2, \ldots, n$, the MLS approximation $u_h^{(k)}(\mathbf{x})$ of $u^{(k)}$, $\forall \mathbf{x} \in \Omega_{\mathbf{x}}$, can be defined as

$$u_h^{(k)}(\mathbf{x}) = \mathbf{p}^T(\mathbf{x})\mathbf{a}^{(k)}(\mathbf{x}), \quad \forall \mathbf{x} \in \Omega_{\mathbf{x}}, \tag{3.1}$$

where $\mathbf{p}^T(\mathbf{x}) = [p_1(\mathbf{x}), p_2(\mathbf{x}), \ldots, p_m(\mathbf{x})]$ is a complete monomial basis of order m, and $\mathbf{a}^{(k)}(\mathbf{x})$ is a vector with components $a_j^{(k)}(\mathbf{x})$, $j = 1, 2, \ldots, m$, which are functions of the space coordinates $\mathbf{x}$. For example, for a two-dimensional problem, the linear basis is: $\mathbf{p}^T(\mathbf{x}) = [1, x, y]$, and the quadratic basis is $\mathbf{p}^T(\mathbf{x}) = [1, x, y, x^2, xy, y^2]$, where $\mathbf{x} = (x, y)$.

The coefficient vector $\mathbf{a}^{(k)}(\mathbf{x})$ is determined by minimizing a weight discrete L_2 norm, which is defined as

$$J^{(k)}(\mathbf{x}) = \sum_{i=1}^{n} w_i(\mathbf{x}) \left[\mathbf{p}^T(\mathbf{x}^i)\mathbf{a}^{(k)}(\mathbf{x}) - \widehat{u}_i^{(k)}\right]^2 = \left[\mathrm{P}\cdot\mathbf{a}^{(k)}(\mathbf{x}) - \widehat{\mathbf{u}}^{(k)}\right]^T \cdot \mathrm{W} \cdot \left[\mathrm{P}\cdot\mathbf{a}^{(k)}(\mathbf{x}) - \widehat{\mathbf{u}}^{(k)}\right], \tag{3.2}$$

where $w_i(\mathbf{x})$ is the weight function associate with the node i. n is the number of nodes in $\Omega_{\mathbf{x}}$ for which the weight function $w_i(\mathbf{x}) > 0$ and $\widehat{u}_i^{(k)}$ are the fictitious nodal values, but not the nodal values of the unknown trial function $u_h^{(k)}(\mathbf{x})$. The matrices P and W are defined as

$$\mathrm{P} = \begin{bmatrix} \mathbf{p}^T(\mathbf{x}^1) \\ \mathbf{p}^T(\mathbf{x}^2) \\ \vdots \\ \mathbf{p}^T(\mathbf{x}^n) \end{bmatrix}_{n\times m}, \qquad \mathrm{W} = \begin{bmatrix} w_1(\mathbf{x}) & \cdots & 0 \\ \cdots & \ddots & \cdots \\ 0 & \cdots & w_n(\mathbf{x}) \end{bmatrix}_{n\times n}.$$

The stationarity point of J, in Eq. (3.2), with respect to $\mathbf{a}^{(k)}(\mathbf{x})$ leads to the following linear relation between $\mathbf{a}^{(k)}(\mathbf{x})$ and $\widehat{\mathbf{u}}^{(k)}$

$$A(\mathbf{x})\mathbf{a}^{(k)}(\mathbf{x}) = B(\mathbf{x})\widehat{\mathbf{u}}^{(k)}, \tag{3.3}$$

where the matrices $A(\mathbf{x})$ and $B(\mathbf{x})$ are defined by

$$A(\mathbf{x}) = \mathrm{P}^T \mathrm{W} \mathrm{P} = B(\mathbf{x})\mathrm{P} = \sum_{i=1}^{n} w_i(\mathbf{x})\mathbf{p}(\mathbf{x}^i)\mathbf{p}^T(\mathbf{x}^i), \tag{3.4}$$

$$B(\mathbf{x}) = \mathrm{P}^T \mathrm{W} = \left[w_1(\mathbf{x})\mathbf{p}(\mathbf{x}^1), w_2(\mathbf{x})\mathbf{p}(\mathbf{x}^2), \ldots, w_n(\mathbf{x})\mathbf{p}(\mathbf{x}^n)\right]. \tag{3.5}$$

The matrix A is often called the moment matrix, it is of size $m \times m$. The MLS approximation is well-defined only when the moment matrix A is non-singular. It can be seen that this is the case if and only if the rank of P equals m. A necessary condition for a well-defined MLS approximation is that at least m weight functions are non-zero, i.e., $n > m$ for each sample point $\mathbf{x} \in \Omega$.

Computing $\mathbf{a}^{(k)}(\mathbf{x})$ using Eq. (3.3) and substituting it into Eq. (3.1), give

$$u_h^{(k)}(\mathbf{x}) = \Phi^T(\mathbf{x}).\widehat{\mathbf{u}}^{(k)} = \sum_{i=1}^{n} \phi_i(\mathbf{x})\widehat{u}_i^{(k)}, \quad \mathbf{x} \in \Omega_{\mathbf{x}}, \tag{3.6}$$

where

$$\Phi^T(\mathbf{x}) = \mathbf{p}^T(\mathbf{x})A^{-1}(\mathbf{x})B(\mathbf{x}), \tag{3.7}$$

or

$$\phi_i(\mathbf{x}) = \sum_{j=1}^{m} p_j(\mathbf{x}) \left[A^{-1}(\mathbf{x})B(\mathbf{x})\right]_{ji}. \tag{3.8}$$

$\phi_i(\mathbf{x})$ is called the shape function of the MLS approximation, corresponding to nodal point $\mathbf{y}^i$. If $w_i(\mathbf{x}) \in C^l(\Omega)$ and $p_j(\mathbf{x}) \in C^s(\Omega)$, $i = 1, 2, \ldots, n, j = 1, 2, \ldots, m$, then $\phi_i(\mathbf{x}) \in C^r(\Omega)$ with $r = \min(l, s)$. The partial derivatives of $\phi_i(\mathbf{x})$ are obtained as

$$\phi_{i,l} = \sum_{j=1}^{m} \left(p_{j,l}[A^{-1}B]_{ji} + p_j[A^{-1}B_{,l} + A^{-1}_{,l}B]_{ji}\right), \tag{3.9}$$

where $A^{-1}_{,l} = (A^{-1})_{,l}$ represents the derivative of the inverse of A with respect to $x_l = x$ (or y), which is given by

$$A^{-1}_{,l} = -A^{-1}A_{,l}A^{-1}, \tag{3.10}$$

where, $(\,)_{,l}$ denotes $\partial(\,)/\partial x_l$. Therefore we can write

$$u_{h,l}^{(k)}(\mathbf{x}) = \sum_{i=1}^{n} \phi_{i,l}(\mathbf{x})\widehat{u}_i^{(k)}, \quad \mathbf{x} \in \Omega_{\mathbf{x}}. \tag{3.11}$$

The Gaussian weight function is applied in the present work as

$$w_i(\mathbf{x}) = \begin{cases} \dfrac{\exp[-(d_i/c_i)^2] - \exp[-(r_i/c_i)^2]}{1 - \exp[-(r_i/c_i)^2]} & 0 \le d_i \le r_i, \\ 0 & d_i > r_i, \end{cases} \tag{3.12}$$

where $d_i = \|\mathbf{x} - \mathbf{x}^i\|$, c_i is a constant controlling the shape of the weight function w_i and r_i is the size of the support domain. This size should be large enough to accommodate a sufficiently large number of nodes covered in the domain of definition of every sample point ($n > m$) to ensure the regularity of the matrix A.

4. Numerical implementation

4.1. Discretized equations

Consider N nodal points on the domain of problem. Some of them being distributed across the global boundary $\partial\Omega$. Eqs. (3.6) and (3.11), imply that the quantities $u^{(k)}$ and $u^{(k)}_{,l}$ can be approximated by the fictitious nodal values $\widehat{u}_i^{(k)}$. For the interior points, substituting the approximation formulae (3.6) and (3.11) into the local integral equation (2.6) yield

$$\begin{aligned} &\frac{1}{3}\sum_{j=1}^{n}\left[\int_{\partial\Omega_s^i}\phi_{j,l}(\mathbf{x})n_l\mathrm{d}\Gamma - 3(\eta+\alpha)\int_{\Omega_s^i}\phi_j(\mathbf{x})\mathrm{d}\Omega\right]\widehat{u}_j^{(k+1)} = -\frac{1}{3}\sum_{j=1}^{n}\left[\int_{\partial\Omega_s^i}\phi_{j,l}(\mathbf{x})n_l\mathrm{d}\Gamma + 6\alpha\int_{\Omega_s^i}\phi_j(\mathbf{x})\mathrm{d}\Omega\right]\widehat{u}_j^{(k)} \\ &\quad - \frac{1}{3}\sum_{j=1}^{n}\left[\int_{\partial\Omega_s^i}\phi_{j,l}(\mathbf{x})n_l\mathrm{d}\Gamma + 3(\eta-\alpha)\int_{\Omega_s^i}\phi_j(\mathbf{x})\mathrm{d}\Omega\right]\widehat{u}_j^{(k-1)} + \int_{\Omega_s^i}\psi(\mathbf{x})\sin(\widetilde{u})\mathrm{d}\Omega, \end{aligned} \tag{4.1}$$

where Ω_s^i is a local sub-domain associated with the point i, i.e. it is a circle centered at $\mathbf{x}^i$ of radius r_0.

Before writing the local integral equation for boundary nodes, the boundary condition can be easily imposed. As can be seen from (1.2), a zero gradient along the boundary Γ must be applied. Therefore in Eq. (2.7) we have

$$\int_{\Gamma_s^i} u_{,l}^{(k+1)} n_l \mathrm{d}\Gamma = \int_{\Gamma_s^i} u_{,l}^{(k)} n_l \mathrm{d}\Gamma = \int_{\Gamma_s^i} u_{,l}^{(k-1)} n_l \mathrm{d}\Gamma = 0.$$

Consequently, for the boundary points, substituting the approximation formulae (3.6) and (3.11) into the local integral equation (2.7) yield

$$\frac{1}{3}\sum_{j=1}^{n}\left[\int_{L_s^i}\phi_{j,l}(\mathbf{x})n_l\mathrm{d}\Gamma - 3(\eta+\alpha)\int_{\Omega_s^{ri}}\phi_j(\mathbf{x})\mathrm{d}\Omega\right]\widehat{u}_j^{(k+1)} = -\frac{1}{3}\sum_{j=1}^{n}\left[\int_{L_s^i}\phi_{j,l}(\mathbf{x})n_l\mathrm{d}\Gamma + 6\alpha\int_{\Omega_s^{ri}}\phi_j(\mathbf{x})\mathrm{d}\Omega\right]\widehat{u}_j^{(k)}$$
$$-\frac{1}{3}\sum_{j=1}^{n}\left[\int_{L_s^i}\phi_{j,l}(\mathbf{x})n_l\mathrm{d}\Gamma + 3(\eta-\alpha)\int_{\Omega_s^{ri}}\phi_j(\mathbf{x})\mathrm{d}\Omega\right]\widehat{u}_j^{(k-1)} + \int_{\Omega_s^{ri}}\psi(\mathbf{x})\sin(\widetilde{u})\mathrm{d}\Omega. \tag{4.2}$$

Combining Eqs. (4.1) and (4.2) and doing the numerical integrations lead to the following N by N system,

$$A\widehat{\mathbf{u}}^{(k+1)} = B\widehat{\mathbf{u}}^{(k)} + C\widehat{\mathbf{u}}^{(k-1)} + D\sin(\widetilde{\mathbf{u}}), \tag{4.3}$$

where $\widehat{\mathbf{u}} = [\widehat{u}_1, \widehat{u}_2, \ldots, \widehat{u}_N]^T$ and D is a diagonal matrix in spite of A, B and C. Solving the system (4.3) leads to numerical solution of the unknown function u at nodal points. But before that, a predictor–corrector scheme must be explained to calculate the approximate vector $\widetilde{\mathbf{u}}$.

4.2. A simple predictor–corrector scheme

As mentioned before, Eqs. (4.1) and (4.2) constitute the N by N algebraic system (4.3) in each time level. At the first time level, i.e. when $k = 0$, $\widehat{\mathbf{u}}^{(0)}$ is determined from the initial condition (1.3), i.e.

$$\widehat{\mathbf{u}}^{(0)} = \mathbf{f},$$

and $\widehat{\mathbf{u}}^{(-1)}$ from the initial condition (1.4), i.e.

$$\widehat{\mathbf{u}}^{(-1)} \simeq \widehat{\mathbf{u}}^{(1)} - 2\Delta t\mathbf{g},$$

where $\mathbf{f} = [f(\mathbf{x}^1), f(\mathbf{x}^2), \ldots, f(\mathbf{x}^N)]^T$ and $\mathbf{g} = [g(\mathbf{x}^1), g(\mathbf{x}^2), \ldots, g(\mathbf{x}^N)]^T$. For dealing with the non-linearity, in each time level (for example time level $k+1$), at first we put

$$\widetilde{\mathbf{u}} = \widehat{\mathbf{u}}^{(k)}.$$

Having this, Eq. (4.3) is solved as a system of linear algebraic equations for unknown $\widehat{\mathbf{u}}^{(k+1)} = \widehat{\mathbf{u}}^{(k+1),0}$. Recompute

$$\widetilde{\mathbf{u}} = \frac{1}{3}\left[\widehat{\mathbf{u}}^{(k+1),0} + \widehat{\mathbf{u}}^{(k)} + \widehat{\mathbf{u}}^{(k-1)}\right].$$

Now Eq. (4.3) is solved using the new $\widetilde{\mathbf{u}}$ for unknown $\widehat{\mathbf{u}}^{(k+1),1}$. We are at time level $k+1$ yet, and iterate between calculating $\widetilde{\mathbf{u}}$ and computing the approximation values of the unknown $\widehat{\mathbf{u}}^{(k+1),l}$ and putting

$$\widetilde{\mathbf{u}} = \frac{1}{3}\left[\widehat{\mathbf{u}}^{(k+1),l} + \widehat{\mathbf{u}}^{(k)} + \widehat{\mathbf{u}}^{(k-1)}\right],$$

until the unknown quantity converge to within a prescribed number of significant figure. For example we can used the following condition for stopping the iterations in each time level,

$$\|\widehat{\mathbf{u}}^{(k+1),l} - \widehat{\mathbf{u}}^{(k+1),l-1}\| \leq \varepsilon,$$

where ε is a fixed number. When this condition is satisfied we can put

$$\widehat{\mathbf{u}}^{(k+1)} = \widehat{\mathbf{u}}^{(k+1),l},$$

and go a head to the next time level. This process is iterated, until reaching to the desirable time t.

Remark. Matrix A defined in (4.3) is constant in all iterations. The algorithm takes advantage of this property. The LU decomposition is performed only once at the beginning of calculations. From there on, the solution of the linearized system (4.3) only requires an update of the right-hand side and a forward and backward substitution to obtained the solution.

4.3. Numerical integrations

Here some explanations are outlined for numerical integrations in Eqs. (4.1) and (4.2). All integrals are regular and no special quadrature need to calculate them. The 16 points Gauss–Legendre quadrature rule is used for numerical integration in all cases.

The first integral in (4.1) is a boundary integral and is calculated as following

$$\begin{aligned}\int_{\partial\Omega_s^i}\phi_{j,l}(\mathbf{x})n_l\mathrm{d}\Gamma &= \int_0^{2\pi}\phi_{j,l}(x^i+r_0\cos\theta, y^i+r_0\sin\theta)n_l r_0\mathrm{d}\theta\\ &= \pi r_0\int_{-1}^{1}\phi_{j,l}(x^i+r_0\cos(\pi\theta+\pi), y^i+r_0\sin(\pi\theta+\pi))n_l\mathrm{d}\theta\\ &\simeq \pi r_0\sum_{p=1}^{16}w_p\left[\frac{\partial\phi_j}{\partial x}(x_p^i,y_p^i)n_1^p+\frac{\partial\phi_j}{\partial y}(x_p^i,y_p^i)n_2^p\right],\end{aligned}$$

where

$$\begin{aligned}x_p^i &= x^i+r_0\cos(\pi\theta_p+\pi)=x^i-r_0\cos(\pi\theta_p),\\ y_p^i &= y^i+r_0\sin(\pi\theta_p+\pi)=y^i-r_0\sin(\pi\theta_p),\end{aligned}$$

and $n^p=(n_1^p,n_2^p)$ is the unit outward vector to $\partial\Omega_s^i$ at point (x_p^i,y_p^i), i.e. $n^p=[-\cos(\pi\theta_p),-\sin(\pi\theta_p)]$.

The second integral in (4.1) is a domain integral and can be calculated as

$$\begin{aligned}\int_{\Omega_s^i}\phi_j(\mathbf{x})\mathrm{d}\Omega &= \int_0^{2\pi}\int_0^{r_0}r\phi_j(x^i+r\cos\theta, y^i+r\sin\theta)\mathrm{d}r\mathrm{d}\theta\\ &= \pi\frac{r_0^2}{4}\int_{-1}^{1}\int_{-1}^{1}(r+1)\phi_j\left(x^i-\frac{r_0}{2}(r+1)\cos(\pi\theta), y^i-\frac{r_0}{2}(r+1)\sin(\pi\theta)\right)\mathrm{d}r\mathrm{d}\theta\\ &\simeq \pi\frac{r_0^2}{4}\sum_{p=1}^{16}\sum_{q=1}^{16}w_pw_q(r_q+1)\phi_j(x_{pq}^i,y_{pq}^i),\end{aligned}$$

where

$$\begin{aligned}x_{pq}^i &= x^i-\frac{r_0}{2}(r_q+1)\cos(\pi\theta_p),\\ y_{pq}^i &= y^i-\frac{r_0}{2}(r_q+1)\sin(\pi\theta_p)\end{aligned}$$

$\{w_p\}$ and $\{\theta_p\}$ [or $\{w_q\}$ and $\{r_q\}$] are the weights and coefficients for regular Gauss–Legendre quadrature rule for integration on $[-1,1]$.

The latest integral in (4.1) treats as same as above domain integral with only difference being ϕ_j replacing by ψ.

Numerical integrations on L_s^i and $\Omega_s'^i$ in Eq. (4.2) are obtained similarly by a change for the bounds of variable θ.

5. Numerical results and discussions

The proposed MLPG scheme is applied to various cases involving two-dimensional line and ring solitons. The examples are chosen for comparison with the results of [23,34,35,24,36,37,26,39] for undamped and damped equations. We need to iterate between finding an estimation for $\widetilde{\mathbf{u}}$ and solving the system (4.3) for a new $\mathbf{u}$ that described in previous section. In all the cases considered, the tolerance number ε is selected as 10^{-5}. Convergence was achieved after less than 6 iteration in all cases tested. Also in all problems the regular node distribution is used and $r_0=0.71\delta$, where δ is the distance between two consecutive nodes in x or y direction (why 0.71δ? Since the union of sub-domains must cover the whole global domain, note that 0.70δ does not ensure this condition). Also $c_i=0.6\delta$, $r_i=4r_0$ and $\Delta t=0.2$ are chosen. The routine has written in VISUAL FORTRAN 6.1 and has done on a Pentium IV laptop PC with a 2.0 GHz CPU and 1 GB RAM.

It is known that, when $\beta=0$, for the SG equation the energy given by the following expression

$$E=E(t)=\frac{1}{2}\int\int\left[u_x^2+u_y^2+u_t^2+2(1-\cos u)\right]\mathrm{d}x\mathrm{d}y, \tag{5.1}$$

is conserved [24,36,25,32,39]. We also investigate this property of SG equation. The evaluation of E are performed using the composite trapezoidal rule for integration.

5.1. Superposition of two orthogonal line solitons

The superposition of two orthogonal line solitons will be obtained for the case of $\psi(x,y)=1$ and $\beta=0$, with initial conditions [26]

$$\begin{aligned}f(x,y) &= 4\tan^{-1}\exp(x)+4\tan^{-1}\exp(y),\\ g(x,y) &= 0,\end{aligned} \tag{5.2}$$

Table 1
The energy of the superposition of two orthogonal line solitons when $t \in [0, 7]$.

Time t	Initial [36]	$E(1.0)$	$E(2.0)$	$E(3.0)$	$E(4.0)$	$E(5.0)$	$E(6.0)$	$E(7.0)$
$E(t)$	175.5745	175.2927	175.2761	175.3188	175.3637	175.3899	175.4045	175.6831

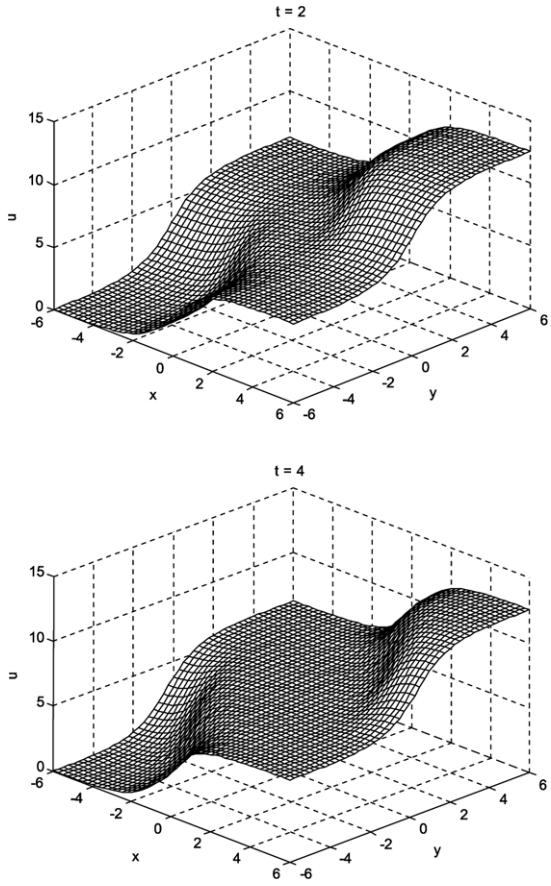

Fig. 2. Superposition of two orthogonal line solitons: Solutions at $t = 2$ and 4.

over the region $-6 \leq x, y \leq 6$. The results are presented in Fig. 2 where the numerical solutions at $t = 2$ and 4 are shown. The results in Fig. 2 show the break up of two orthogonal line solitons which are parallel to the diagonal $y = -x$ and are moving away from each other in the direction of $y = x$, undisturbed. The comparison between the separations at $t = 3, 4$ and $t = 4, 7$ are also depicted in Fig. 3. Let us check the conservation of energy in this case. Table 1 presents the values of $E(t)$ when $\beta = 0$ at some selected times t up to $t = 7$. It is maintained from the relevant contours that until $t = 4$ this separation occurs without any deformation, while at $t = 7$ a deformation has already appeared. The present solutions are in good agreement with the corresponding results of [23,34,35,24,36,26,39]. Also in order to examine the behaviour of the dissipative term, the solution is evaluated at $t = 3$ when $\beta = 0, 0.5$ and 1.5. The resulting solitons are shown in Fig. 4 when full contours show the solitons when $\beta = 0$, while the dashed ones when $\beta = 0.5$ and 1.5. As can be seen from this figure, the presence of the dissipative term delays the propagation of the solitons. This delay becomes obvious when the larger value of β ($\beta = 1.5$) is used. This conclusion agrees with [24,39].
Note that these solutions are calculated using $\delta = 0.25$, i.e. using 2401 nodal points. The CPU time needed to reach $t = 7$ is 166 s using above-mentioned computer and double-precision arithmetic.

5.2. Perturbation of a line soliton

A static line soliton is perturbed to produce two symmetric dents moving towards each other with a constant unit velocity. According to [23,24,26] the dents collide and continue with the same velocity and no shift occurs. Perturbation of a single soliton has been calculated for $\beta = 0$ and $\psi(x, y) = 1$, in terms of $\sin(u/2)$ at $t = 0, 2, 5, 7, 9$ and 11 with the initial

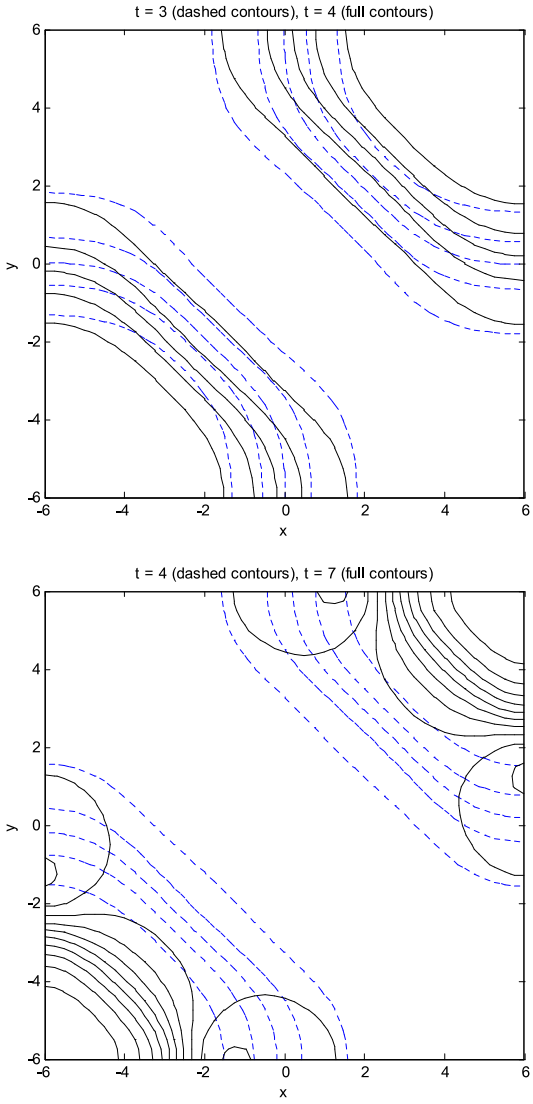

Fig. 3. Comparison of superposition of two orthogonal line solitons at $t = 3$, 4 and 7.

Table 2
The energy of the perturbation of a soliton when $t \in [0, 11]$.

Time t	Initial	$t = 2$	$t = 5$	$t = 7$	$t = 9$	$t = 11$
$E(t)$	122.6648	122.0077	121.9533	122.0111	122.0466	121.9352

conditions

$$\begin{aligned} f(x, y) &= 4\tan^{-1}\exp\left[x + 1 - 2\,\mathrm{sech}(y + 7) - 2\,\mathrm{sech}(y - 7)\right], \\ g(x, y) &= 0, \end{aligned} \tag{5.3}$$

over the region $-7 \leq x, y \leq 7$. The results in Fig. 5 show two symmetric dents moving toward each other, collapsing at $t = 7$ and continuing to move away from each other thereafter. It can be deduced that after the collision the dents retain their shape, which confirms the conclusions of [23,24,26,38,25,39]. Table 2 presents the values of $E(t)$ at some selected times t, that shows the energy remains constant as time increases.

Note that the computations carried out for $\delta = 0.25$, i.e. 3249 scattering nodal points. The CPU time needed to reach $t = 11$ is 324 s.

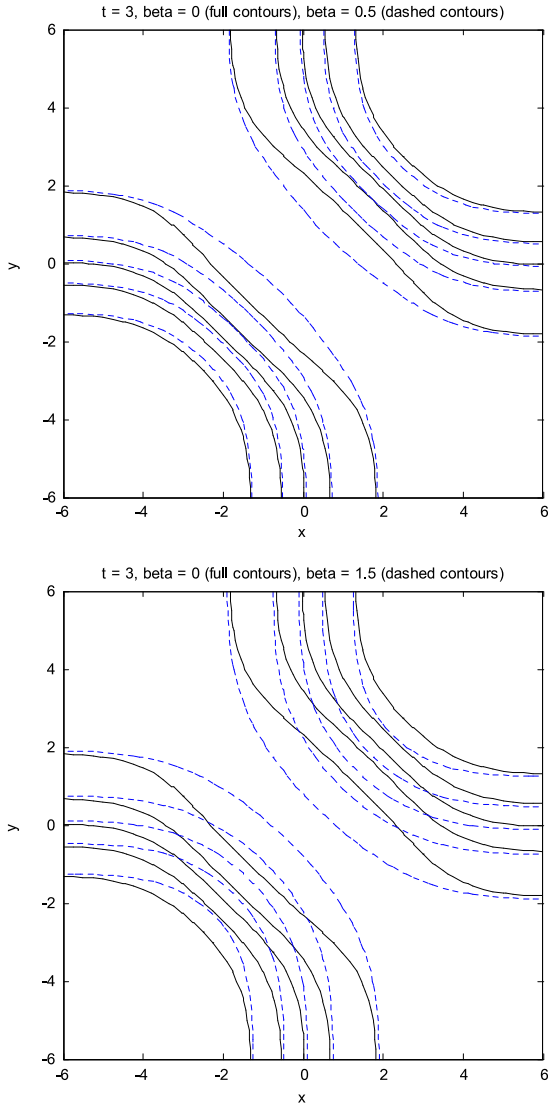

Fig. 4. Comparison of superposition of two orthogonal line solitons at $t = 3$ for $\beta = 0$, 0.5 and 1.5.

5.3. Circular ring soliton

The behaviour of a circular ring quasi-soliton arising from the SG equation was investigated numerically in [48,49], who named these waves pulsons because of their pulsating behaviour. Then some studies concerning the behaviour of these quasi-soliton waves have been published in [50–54], etc.

In Fig. 6, circular ring solitons for the case of $\psi(x, y) = 1$, $\beta = 0$ and initial conditions

$$\begin{aligned} f(x, y) &= 4 \tan^{-1} \exp\left[3 - \sqrt{x^2 + y^2}\right], \\ g(x, y) &= 0, \end{aligned} \tag{5.4}$$

over the region $-7 \leq x, y \leq 7$ at time $t = 0$ (initial condition) and the numerical solutions at $t = 2.8$, 5.6, 8.4, 11.2 and 12.6 are shown in terms of $\sin(u/2)$ for corresponding contours. The soliton from its initial position, shrinks until $t = 2.8$ appearing as a single-ring soliton. From $t = 5.6$, which could be considered as the beginning of the expansion phase, a radiation appears, which is followed by oscillations at the boundaries. This expansion is continued until $t = 11.2$, where the soliton is almost reformed. Finally since $t = 12.6$ it appears to be again in its shrinking phase. During all the above transformations no displacement of the center of the soliton occurred.

Table 3 presents the values of $E(t)$ at some selected times t up to 12.6 which shows the energy remains constant as time increases.

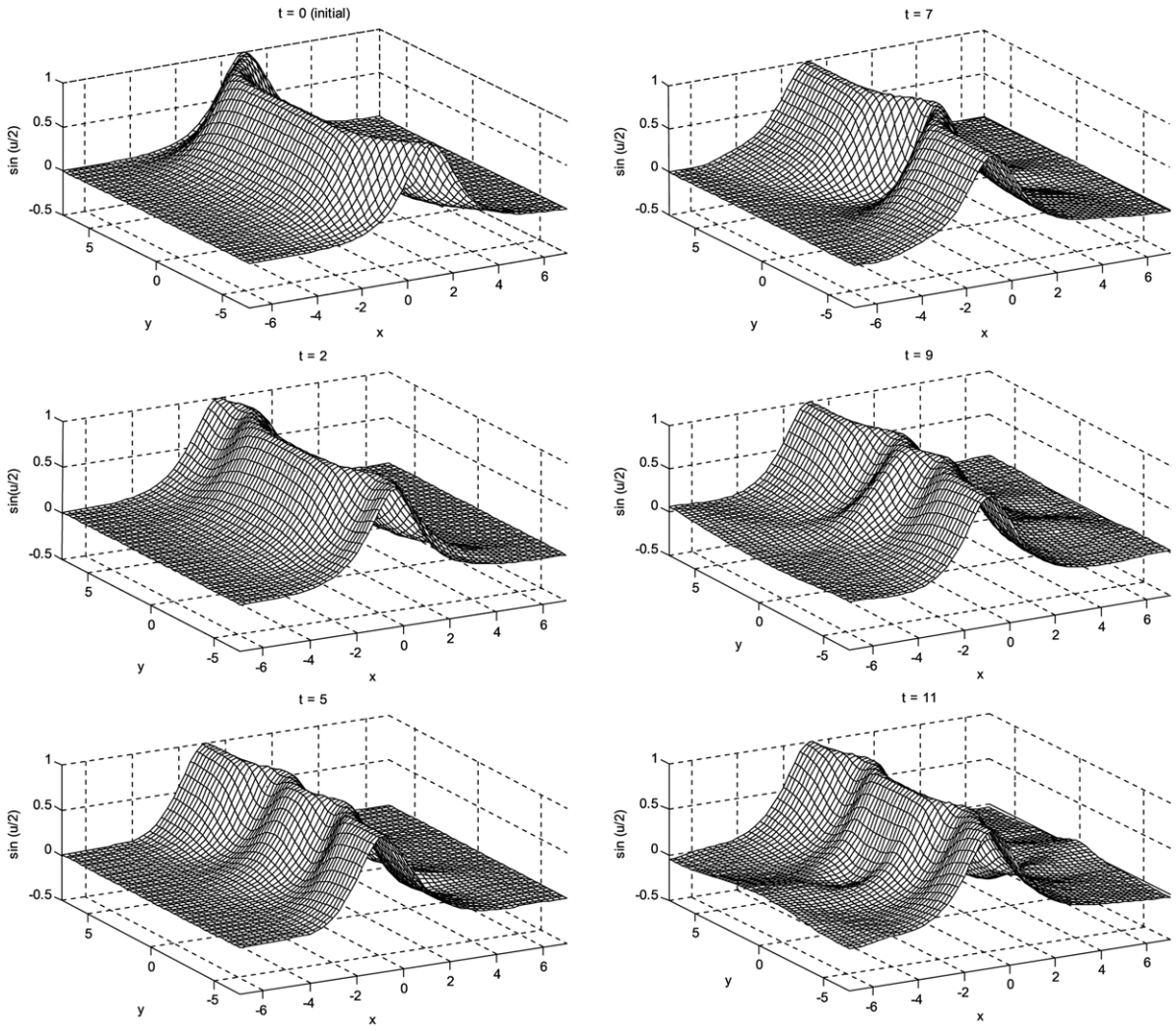

Fig. 5. Perturbation of a line soliton: Solutions at $t = 0, 2, 5, 7, 9$ and 11.

Table 3
The energy $E(t)$ of the circular ring solitons when $t \in [0, 12.6]$.

Time t	Initial [36]	$t = 2.8$	$t = 5.6$	$t = 8.4$	$t = 11.2$	$t = 12.6$
$E(t)$	150.4599	150.4337	150.6655	150.3819	150.9022	150.7613

The present solutions are in good agreement with the corresponding results of [23,34,35,24,36,37,39]. The computations were performed using $\delta = 0.25$, i.e. 3249 scattering regular nodal points. The CPU time required to reach $t = 12.6$ is 333 s.

5.4. Elliptical ring soliton

Elliptical ring solitons are obtained for $\psi(x, y) = 1$ and $\beta = 0$ with initial conditions

$$\begin{aligned} f(x, y) &= 4 \tan^{-1} \exp\left(3 - \sqrt{(x-y)^2/3 + (x+y)^2/2}\right), \\ g(x, y) &= 0, \end{aligned} \tag{5.5}$$

over the region $-7 \leq x, y \leq 7$. The contour plots at times $t = 0$, 1.6, 3.2, 4.8, 6.4, 8.0, 9.6 and 11.2 are shown in Fig. 7, in terms of $\sin(u/2)$. The temporal behaviour of the soliton consists of a shrinking and an expanding phase. The associated

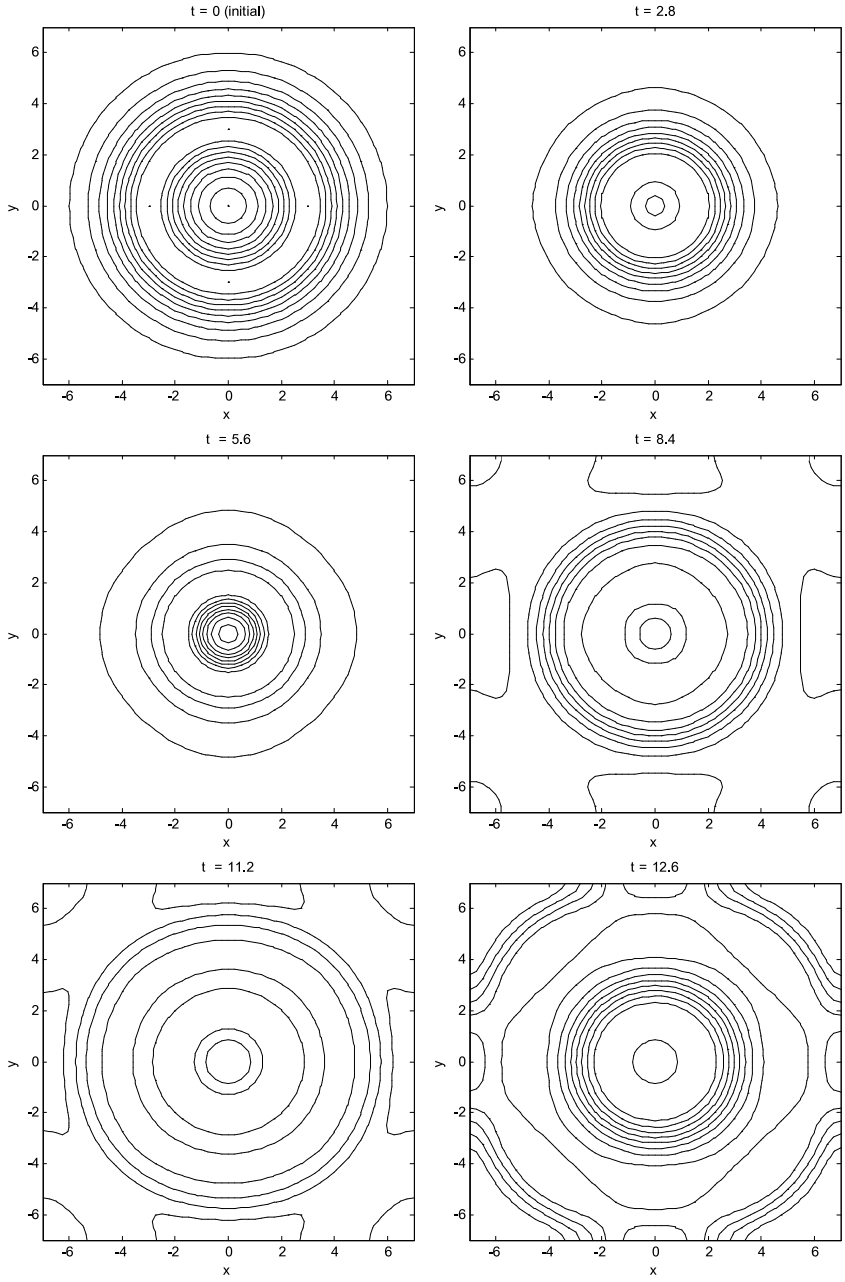

Fig. 6. Circular ring solitons: Solutions at $t = 0$, 2.8, 5.6, 8.4, 11.2 and 12.6.

Table 4
The energy of the elliptical ring solitons when $t \in [0, 11.2]$.

Time t	Initial	$t = 1.6$	$t = 3.2$	$t = 4.8$	$t = 6.4$	$t = 8.0$	$t = 9.6$	$t = 11.2$
$E(t)$	169.1214	168.6101	168.6710	168.8143	168.7978	169.3887	169.5619	169.4832

pulsation of the wave is accompanied by a permanent change in the orientation of the major and minor axes of the ellipse. At $t = 11.2$, an essentially circular ring soliton are seen [23,24]. These results are in good agreement with those given in [23,24,38,39]. Table 4 presents the values of $E(t)$ when $\beta = 0$ at some selected times t up to $t = 11.2$. The results were performed using $\delta = 0.25$, i.e. 3249 scattering regular nodal points. The CPU time required to reach $t = 11.2$ is 325 s.

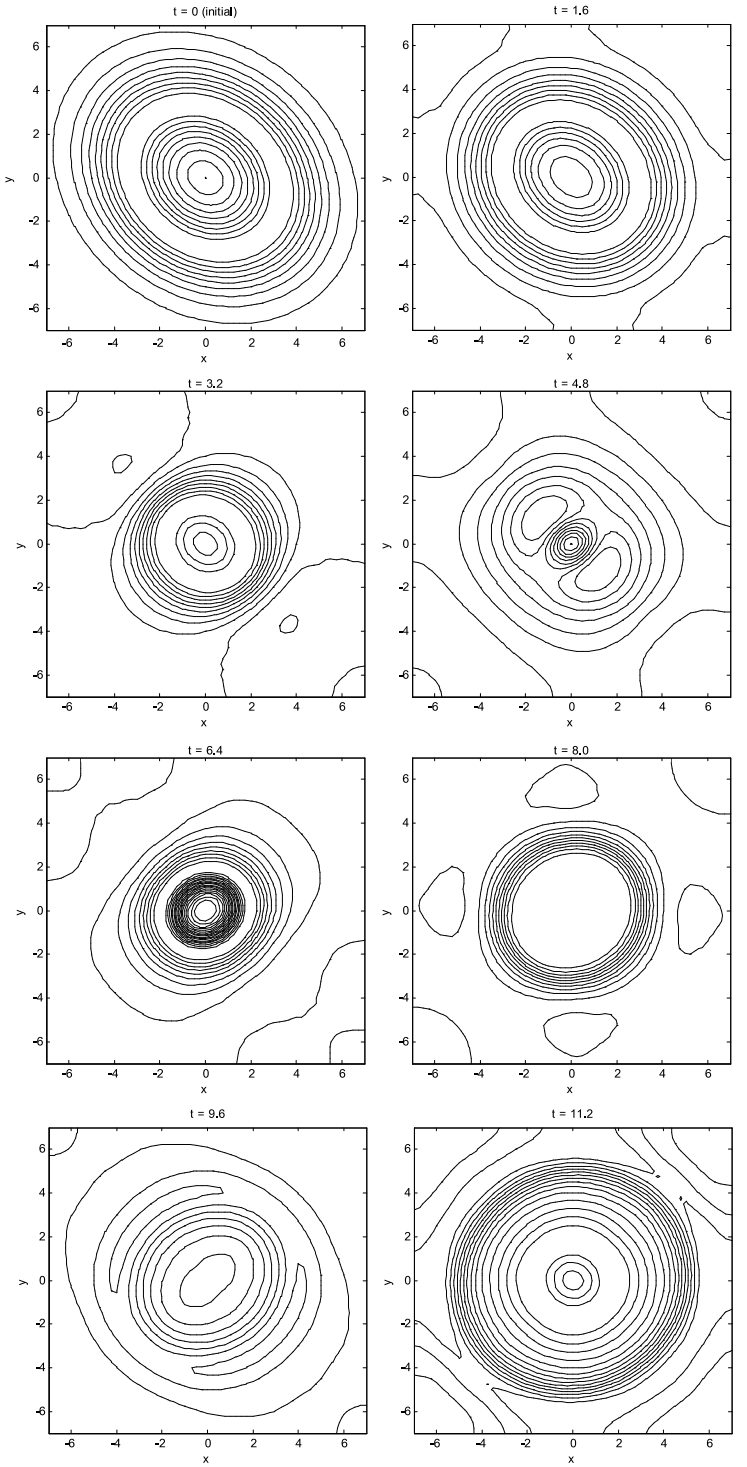

Fig. 7. Elliptical ring solitons: Solutions at $t = 0$, 1.6, 3.2, 4.8, 6.4, 8.0, 9.6 and 11.2.

5.5. Elliptical breather

An elliptical breather [48] is obtained for $\psi(x, y) = 1$ with initial conditions [26],

$$\begin{aligned} f(x, y) &= 4\tan^{-1}\left[2.0\,\mathrm{sech}\left[0.866\sqrt{(x-y)^2/3 + (x+y)^2/2}\right]\right], \\ g(x, y) &= 0, \end{aligned} \tag{5.6}$$

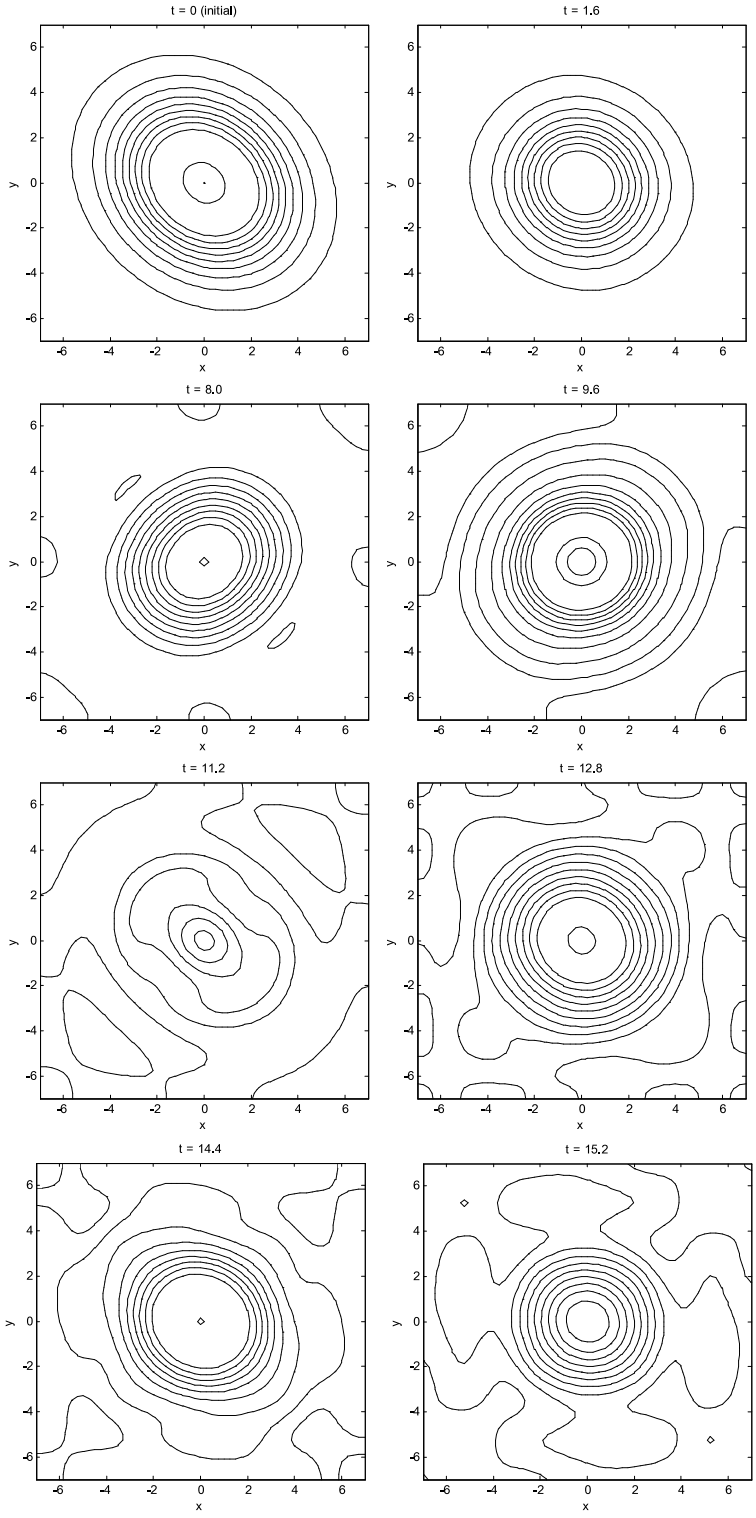

Fig. 8. Elliptical breather: Solutions at $t = 0$, 1.6, 8.0, 9.6, 11.2, 12.8, 14.4 and 15.2.

over the region $-7 \leq x, y \leq 7$. In Fig. 8 the contours of the elliptical breather at $t = 0$, 1.6, 8, 9.6, 11.2, 12.8, 14.4 and 15.2 are given when $\beta = 0$. The major axes of the breather from its initial direction $y = x$ seems to be turned clockwise shrinking until $t = 1.6$, while at $t = 8$ and 9.6 a reflexion phase is observed. At $t = 11.2$ the major axes has almost recovered its initial direction ($y = x$), but strong oscillations are observed [24,36]. After $t = 12.8$ an expansion phase is observed. The

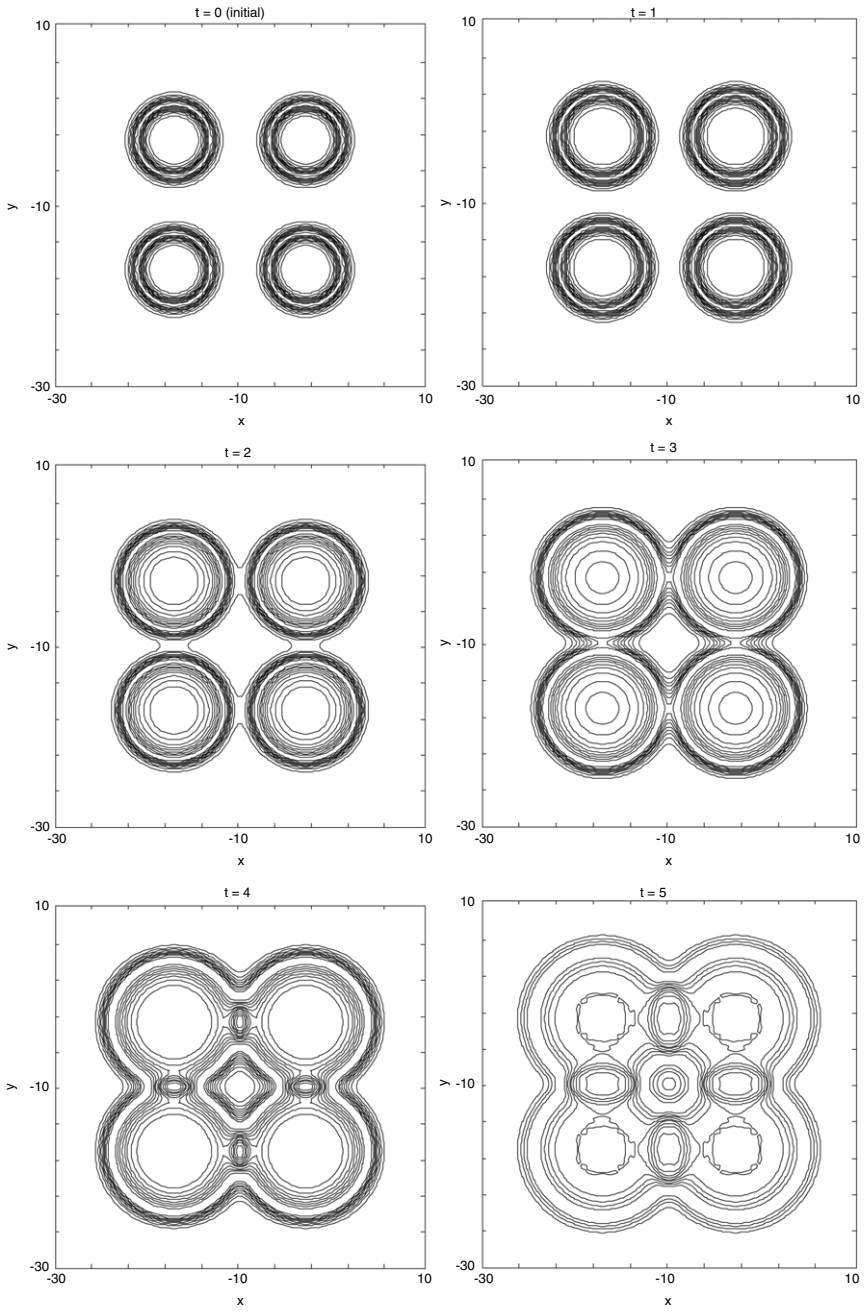

Fig. 9. Collision of four circular ring solitons: Solutions at $t = 0, 1, 2, 3, 4, 5, 6, 7, 8, 9, 10$ and 11.

Table 5
The energy of the elliptical breather when $t \in [0, 15.2]$.

Time t	Initial [36]	$t = 1.6$	$t = 8.0$	$t = 9.6$	$t = 11.2$	$t = 12.8$	$t = 14.4$	$t = 15.2$
$E(t)$	89.6761	89.6812	89.6612	89.4257	89.0125	89.6545	89.6085	89.7432

graphs are in agreement with those given in [23,34,24,36,39]. As previous, Table 5 shows that the energy remains constant as time increases. The results were calculated using $\delta = 0.25$, i.e. 3249 scattering regular nodal points. The CPU time needed to reach $t = 15.2$ is 340 s.

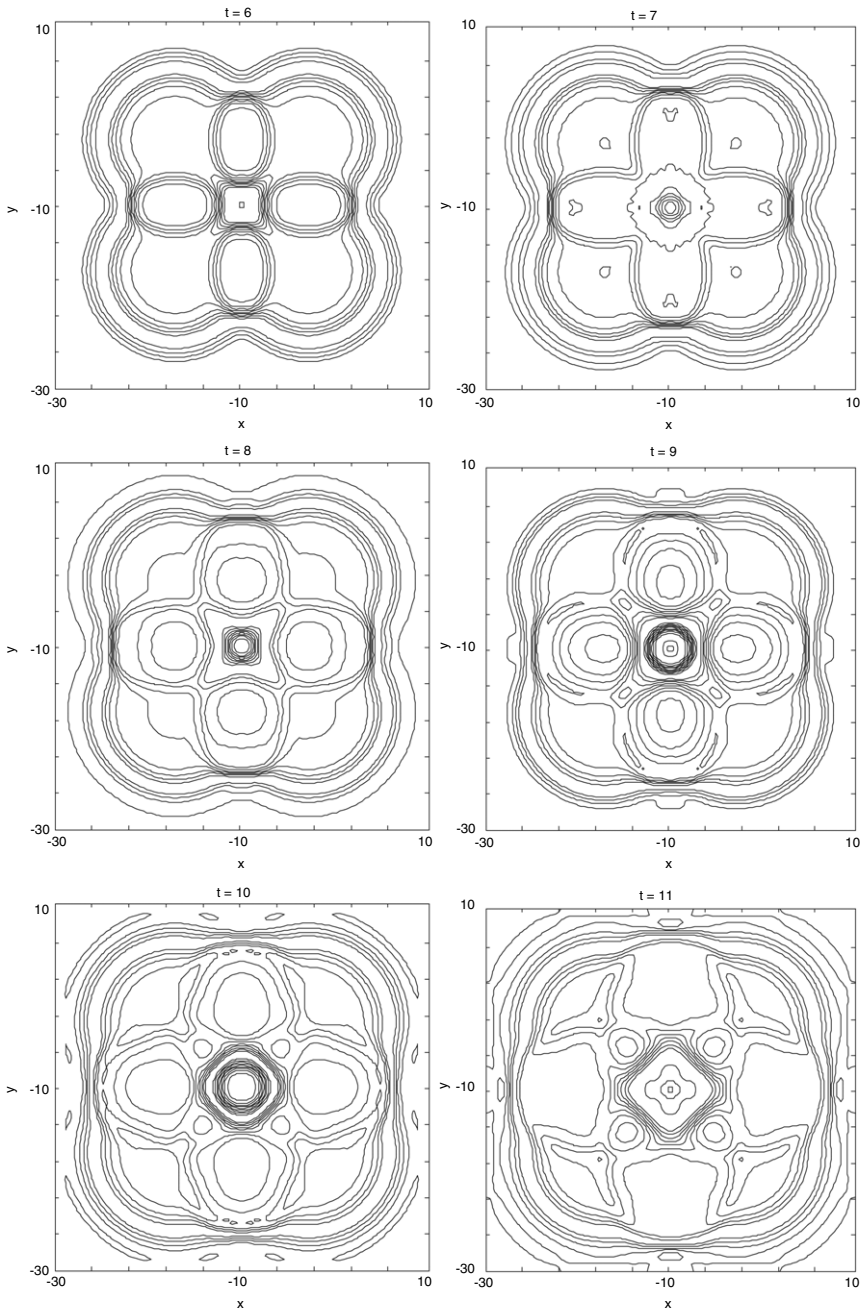

Fig. 9. (*continued*)

5.6. Collision of four circular solitons

The collision of four expanding circular ring solitons is considered for $\psi(x, y) = 1$ and initial condition

$$f(x, y) = 4\tan^{-1}\exp\left[\frac{1}{0.436}\left[4 - \sqrt{(x+3)^2 + (y+3)^2}\right]\right],$$
$$g(x, y) = 4.13/\cosh\left[\frac{1}{0.436}\left[4 - \sqrt{(x+3)^2 + (y+3)^2}\right]\right], \tag{5.7}$$

over the region $-30 \leq x, y \leq 10$. For numerical solution we chose $\delta = 0.4$, i.e. 2601 nodal points over one quarter of the domain. The solution is expanded along the sides $x = -10$ and $y = -10$ using the symmetry relations. The

calculation is carried out to $t = 11$ and the corresponding contour plots are depicted in Fig. 9 in terms of $\sin(u/2)$. The results show an extremely complex interaction with rapidly varying values of u in the center and are in excellent agreement with corresponding results given in [23,39]. The CPU time required to reach $t = 11$ is 252 s.

6. Concluding remarks

The meshless local Petrov–Galerkin (MLPG) method formulated and successfully implemented for solving the non-linear two-dimensional sine-Gordon (SG) equation. The analyzed domain divided into small overlapping circular sub-domains. A unit-step function used as the test function in the local weak form. The derived local boundary-domain integral equations were non-singular. The moving least-squares (MLS) scheme adopted for approximating the physical quantities. A time-stepping method employed to deal with the time derivatives and a predictor–corrector scheme presented to eliminate the non-linearity. For SG problem, some numerical experiments involving line and ring solitons, investigated and the reformations of the solitons from initial condition to final time presented. Also to test the accuracy of the proposed method the values of energy at several time-steps computed.

The proposed method is a truly meshless method, which requires neither domain elements nor background cells in either the interpolation or the integration. This is an alternative numerical tool to many existing computational methods. The main advantage is its simplicity. No special computational technique is required to evaluate the integrals. Besides, the present meshless method is more flexible because it allows an easy adaptation of the nodal density. Hence, many existing adaptive algorithms can be applied. Moreover, as demonstrated by the computational results reported in Section 5, the proposed technique is able to deal with the unsteady non-linear problems; thus it is particularly useful for studying the SG equation and other evolution problems in this family.

References

[1] T. Belytschko, Y.Y. Lu, L. Gu, Element-free Galerkin methods, Internat. J. Numer. Methods Engrg. 37 (1994) 229–256.
[2] C.A. Duarte, J.T. Oden, H-p clouds-an hp meshless method, Numer. Methods Partial Differential Equations 12 (1996) 673–705.
[3] W. Liu, S. Jun, Y. Zhang, Reproducing kernel particle method, Internat. J. Numer. Methods Fluids 20 (1995) 1081–1106.
[4] L.B. Lucy, A numerical approach to the testing of the fission hypothesis, Astron. J. 82 (12) (1977) 1013–1024.
[5] B. Nayroles, G. Touzot, P. Villon, Generalizing the finite element method: Diffuse approximation and diffuse elements, Comput. Mech. 10 (1992) 307–318.
[6] J.M. Melenk, I. Babuska, The partition of unity finite element method: Basic theory and applications, Comput. Methods Appl. Mech. Engrg. 139 (1996) 289–314.
[7] N. Sukumar, B. Moran, T. Belytschko, The natural element method in solid mechanics, Internat. J. Numer. Methods Engrg. 43 (1998) 839–887.
[8] P. Lancaster, K. Salkauskas, Surfaces generated by moving least squares methods, Math. Comp. 37 (1981) 141–158.
[9] S.N. Atluri, T. Zhu, A new meshless local Petrov–Galerkin (MLPG) approach in computational mechanics, Comput. Mech. 22 (2) (1998) 117–127.
[10] S.N. Atluri, S.P. Shen, The meshless local Petrov–Galerkin (MLPG) method: A simple and less-costly alternative to the finite element methods, Comput. Model. Eng. Sci. 3 (1) (2002) 11–51.
[11] S.N. Atluri, The Meshless Method (MLPG) for Domain and BIE Discretizations, Tech Science Press, 2004.
[12] R.C. Batra, M. Porfiri, D. Spinello, Treatment of material discontinuity in two meshless local Petrov–Galerkin (MLPG) formulations of axisymmetric transient heat conduction, Internat. J. Numer. Methods Engrg. 61 (2004) 2461–2479.
[13] M. Dehghan, D. Mirzaei, The meshless local Petrov–Galerkin (MLPG) method for the generalized two-dimensional non-linear Schrödinger equation, Eng. Anal. Bound. Elem. 32 (2008) 747–756.
[14] M. Dehghan, D. Mirzaei, Meshless Local Petrov–Galerkin (MLPG) method for the unsteady magnetohydrodynamic (MHD) flow through pipe with arbitrary wall conductivity, Appl. Numer. Math. 59 (2009) 1043–1058.
[15] J. Sladek, V. Sladek, J. Krivacek, P.H. Wen, Ch. Zhang, Meshless local Petrov–Galerkin (MLPG) method for Reissner–Mindlin plates under dynamic load, Comput. Methods Appl. Mech. Engrg. 196 (2007) 2681–2691.
[16] J. Sladek, V. Sladek, Y.C. Hon, Inverse heat conduction problems by meshless local Petrov–Galerkin method, Eng. Anal. Bound. Elem. 30 (2006) 650–661.
[17] J. Sladek, V. Sladek, Ch. Zhang, M. Schanz, Meshless local Petrov–Galerkin method for continuously nonhomogeneous linear viscoelastic solids, Comput. Mech. 37 (2006) 279–289.
[18] J. Sladek, V. Sladek, Ch. Zhang, J. Krivacek, Ph. Wen, Analysis of orthotropic thick plates by meshless local Petrov–Galerkin (MLPG) method, Internat. J. Numer. Methods Engrg. 67 (2006) 1830–1850.
[19] J.R. Xiao, M.A. McCarthy, Meshless analysis of the obstacle problem for beams by the MLPG method and subdomain variational formulations, Eur. J. Mech. A Solids 22 (2003) 385–399.
[20] M. Dehghan, Finite difference procedures for solving a problem arising in modeling and design of certain optoelectronic devices, Math. Comput. Simulation 71 (2006) 16–30.
[21] N.F. Pedersen, S. Madsen, Search for the in-phase flux flow mode in stacked Josephson junctions, Physica C 437 (2006) 262–266.
[22] H. Susanto Darminto, S.A. van Gils, Static sand dynamic properties of fluxons in a zig-zag 0-π Josephson junction, Phys. Lett. A 361 (2007) 270–276.
[23] J. Argyris, M. Haase, J.C. Heinrich, Finite element approximation to two-dimensional sine-Gordon solitons, Comput. Methods Appl. Mech. Engrg. 86 (1991) 1–26.
[24] A.G. Bratsos, The solution of the two-dimensional sine-Gordon equation using the method of lines, J. Comput. Appl. Math. 206 (2007) 251–277.
[25] K. Djidjeli, W.G. Price, E.H. Twizell, Numerical solutions of a damped sine-Gordon equation in two space variables, J. Engrg. Math. 29 (1995) 347–369.
[26] P.L. Christiansen, P.S. Lomdahl, Numerical solutions of $2 + 1$ dimensional sine-Gordon solitons, Physica D 2 (3) (1981) 482–494.
[27] R. Hirota, Exact three-soliton solution of the two-dimensional sine-Gordon equation, J. Phys. Soc. Japan 35 (1973) 1566.
[28] P.L. Christiansen, O.H. Olsen, Return effect for rotationally symmetric solitary wave solutions to the sine-Gordon equation, Phys. Lett. A 68 (2) (1978) 185–188.
[29] J. Zagrodzinsky, Particular solutions of the sine-Gordon equation in $2 + 1$ dimensions, Phys. Lett. A 72 (1979) 284–286.
[30] P. Kaliappan, M. Lakshmanan, Kadomtsev–Petviashvili and two-dimensional sine-Gordon equations: Reduction to Painlevè transcendents, J. Phys. A: Math. Gen. 12 (1979) L249–L252.
[31] G. Leibbrandt, New exact solutions of the classical sine-Gordon equation in $2 + 1$ and $3 + 1$ dimensions, Phys. Rev. Lett. 41 (1978) 435–438.
[32] B.Y. Guo, P.J. Pascual, M.J. Rodriguez, L. Vázquez, Numerical solution of the sine-Gordon equation, Appl. Math. Comput. 18 (1986) 1–14.
[33] Q. Sheng, A.Q.M. Khaliq, D.A. Voss, Numerical simulation of two-dimensional sine-Gordon solitons via a split cosine scheme, Math. Comput. Simulation 68 (2005) 355–373.

[34] A.G. Bratsos, An explicit numerical scheme for the sine-Gordon equation in 2 + 1 dimensions, Appl. Num. Anal. Comp. Math. 2 (2) (2005) 189–211.
[35] A.G. Bratsos, A modified predictor–corrector scheme for the two-dimensional sine-Gordon equation, Numer. Algorithms 43 (2006) 295–308.
[36] A.G. Bratsos, A third order numerical scheme for the two-dimensional sine-Gordon equation, Math. Comput. Simulation 76 (2007) 271–282.
[37] A.G. Bratsos, An improved numerical scheme for the sine-Gordon equation in 2+1 dimensions, Internat. J. Numer. Methods Engrg. 75 (2008) 787–799.
[38] M. Dehghan, D. Mirzaei, The dual reciprocity boundary element method (DRBEM) for two-dimensional sine-Gordon equation, Comput. Methods Appl. Mech. Engrg. 197 (2008) 476–486.
[39] D. Mirzaei, M. Dehghan, Boundary element solution of the two-dimensional sine-Gordon equation using continuous linear elements, Eng. Anal. Bound. Elem. 33 (2009) 12–24.
[40] M. Dehghan, A. Shokri, A numerical method for solution of the two-dimensional sine-Gordon equation using the radial basis functions, Math. Comput. Simulation 79 (2008) 700–715.
[41] M. Dehghan, D. Mirzaei, The boundary integral equation approach for numerical solution of the one-dimensional sine-Gordon equation, Numer. Methods Partial Differential Equations 24 (2008) 1405–1415.
[42] A.M. Wazwaz, The tanh method and a variable separated ODE method for solving double sine-Gordon equation, Phys. Lett. A 350 (2006) 367–370.
[43] A.M. Wazwaz, Exact solutions for the generalized sine-Gordon and the generalized sinh-Gordon equations, Chaos Solitons Fractals 28 (2006) 127–135.
[44] M.A. Helal, Soliton solution of some nonlinear partial differential equations and its application in fluid mechanics, Chaos Solitons Fractals 13 (2002) 1917–1929.
[45] D.A. Hu, S.Y. Long, K.Y. Liu, G.Y. Li, A modified meshless local Petrov–Galerkin method to elasticity problems in computer modelling and simulation, Eng. Anal. Bound. Elem. 30 (2006) 399–404.
[46] K.Y. Liu, S.Y. Long, G.Y. Li, A simple and less-costly meshless local Petrov–Galerkin (MLPG) method for the dynamic fracture problem, Eng. Anal. Bound. Elem. 30 (2006) 72–76.
[47] T. Belytschko, Y. Krongauz, D. Organ, M. Fleming, P. Krysl, Meshless methods: An overview and recent developments, Comput. Methods Appl. Mech. Engrg. 139 (1996) 3–47.
[48] I.L. Bogolyubskiĭ, V.G. Makhankov, Lifetime of pulsating solitons in certain classical models, JETP Lett. 24 (1) (1976) 12–14.
[49] I.L. Bogolyubskiĭ, Oscillating particle-like solutions of the nonlinear Klein–Gordon equation, JETP Lett. 24 (10) (1976) 535–538.
[50] P.L. Christiansen, N. Grønbech-Jensen, P.S. Lomdahl, B.A. Malomed, Oscillations of eccentric Pulsons, Phys. Scr. 55 (1997) 131–134.
[51] B.A. Malomed, Decay of shrinking solitons in multidimensional sine-Gordon equation, Physica D 24 (1987) 155–171.
[52] B.A. Malomed, Dynamic of quasi-one-dimensional kinks in the two-dimensional sine-Gordon model, Physica D 52 (1991) 157–170.
[53] E.M. Maslov, Dynamics of rotationally symmetric solitons in near-SG field model with applications to large-area Josephson junctions and ferromagnets, Physica D 15 (1985) 433–443.
[54] E.M. Maslov, Rotationally symmetric SG oscillator with tunable frequency, Phys. Lett. A 131 (6) (1988) 364–367.